CrystEngComm

Accepted Manuscript

ROYAL SOCIETY OF CHEMISTRY

www.rsc.org/crystengcomm

Journal Name

RSCPublishing

ARTICLE

Crystal Structure Analysis of Molecular Dynamics using Synchrotron X-rays

Cite this: DOI: 10.1039/x0xx00000x

Manabu Hoshino,*[a] Shin-ichi Adachi[b] and Shin-ya Koshihara[a]

Received 00th January 2012,
Accepted 00th January 2012

DOI: 10.1039/x0xx00000x

www.rsc.org/

The recent development of X-ray crystallography using synchrotron X-rays have made it an improved analytical approach compared with the previously used temporally and spatially averaged observations in an analyte crystal. The short-pulse character of synchrotron X-rays enables conduction of a time-resolved X-ray experiment to observe the temporal three dimensional dynamics in a crystal. This experimental technique is useful for studies regarding the photo-induced phenomena. Additionally, high intensity X-rays from a synchrotron source are effective for investigating thermal dynamics of molecules in a crystal with atomic resolution. In both cases, the dynamic nature of the molecule and molecular aggregation in a crystal are deeply involved in its function as a material. Molecular dynamics of a crystal lead to a change of the physical properties of the crystalline phase. Examples for three-dimensional observations of molecular dynamics with atomic resolution using synchrotron X-ray are summarized.

Physical and chemical phenomena, such as chemical reactions, phase transition, energy conversion and so forth, accompany structural changes of the molecule. Determining the structural dynamics of molecules will provide a detailed understanding about processes and functions concerning the above phenomena. X-ray crystal structure analysis is a powerful tool for the study of the structural features of molecules with atomic resolution. However, observation of the dynamic nature of molecules, using X-ray crystal structure analysis, is not a straightforward task because typical X-ray crystal structure analysis is applied for observation of temporally and spatially averaged molecular structures in a crystal. The structural dynamics induced by photo-excitation is taken as an example. A typical lifetime of a photo-excited molecule is shorter than one millisecond. An X-ray source installed in an in-house diffractometer provides a continuous X-ray beam so that the crystal structure obtained by X-ray structural analysis is averaged over the total accumulation time of the diffraction data collection. Therefore, ultrafast spectroscopy is typically used for studying photo-excited molecules because the short-pulsed intense light derived from a laser is available for probing the vibrational or electronic transitions inherent in a molecule with a short-lived photo-excited state. Pump-probe X-ray crystallography is designed by mimicking ultrafast spectroscopy for the study of the molecular structure of a photo-excited state with atomic resolution.[1-7] In this method, pulsed laser light (a typical pulse width is about 100 fs) is used for excitation of the molecule and is synchronized with an X-ray pulse derived from a synchrotron storage ring (width is approximately 100 ps).[8] Structural deformation by photo-excitation in some molecules has been observed by applying this method.[9-11]

The difficulties in studying thermally induced molecular dynamics by X-ray crystal structure analysis are different from the above. The large movement of the molecules and functional groups by thermal motions significantly decrease the X-ray diffraction intensity, especially at the high-angle region. The absence of high-angle diffraction data in the crystal structure analysis reduces the atomic resolution in the Fourier map and makes a detailed observation of their dynamic thermal motion impossible. This weakly diffracting feature in a crystal containing thermally disturbed molecules is a fundamental nature of their thermal dynamics. Therefore, increasing the diffraction intensities arising from such a crystal is the most simple, but formidable, way to solve this issue. Synchrotron X-rays would be the best choice to use as a source for the diffraction experiment of the above weakly diffracting crystal. The X-ray crystal structure analysis of a tiny (sub-micrometer dimensions) crystal, for which it is generally impossible to obtain a suitable diffraction intensity using an in-house X-ray generator, is an ideal example to demonstrate the efficiency of synchrotron X-rays for weakly diffracting samples.[12,13]

Herein, some X-ray crystallographic studies of photo-[14,15] and thermally-induced[16] molecular dynamics using synchrotron X-rays are reviewed. The first example is a snapshot-style observation of a photo-excited molecule in a crystal. Rearrangement of crystal packing surrounding a photo-excited molecule represents the changing structural and electronic features of a target molecule by photo-excitation. The second example involves the stepwise molecular dynamics described using a sequence of snapshot observations at different synchronized timings of the X-ray and excitation laser pulse in pump-probe X-ray crystallography. The last example involves the thermal dynamics of molecules in a crystal. All examples deal with photo-functional materials. The observed dynamic features of molecules clearly represent their photo-function and provides a solid foundation for their understanding.

Pump-probe X-ray diffraction to observe photo-induced molecular dynamics

In addition to a synchrotron as a source of X-ray pulses and a suite of femtosecond laser systems, many additional instruments and apparatus are required to perform pump-probe X-ray crystallography. Here, the experimental setup for a pump-probe X-ray diffraction experiment at the PF-AR NW14A beamline in KEK,[8] which is where all experiments for the present studies were performed, is described. A simple schematic representing the setup is shown in Fig. 1.

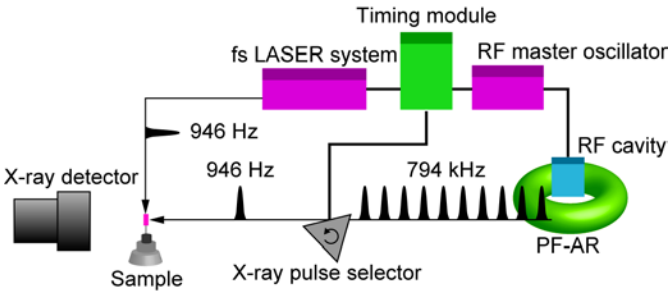

Fig. 1 Simple schematic of the experimental setup for the pump-probe X-ray diffraction experiment at PF-AR NW14A. Reproduced from Ref. 17 with permission from The Surface Science Society of Japan.

Timing of the X-ray pulses was dictated the RF master oscillator, which controls the formation of electron bunches at the RF cavity in the storage ring. The required interval is transferred from the timing module to the femtosecond laser system and the X-ray pulse selector for synchronizing the X-ray and laser pulses at the sample position.[8] The X-ray pulse selector reduces the frequency of the X-ray pulse from 794 kHz to 946 Hz, which is the same as the typical frequency of the femtosecond laser oscillation.

The number of X-ray photons in one X-ray pulse are far from sufficient for collecting suitable diffraction intensity data to perform single crystal X-ray structural analysis. Therefore, the accumulation of diffraction intensity by thousands of repeating X-ray and laser exposure (several tens of seconds or, in some cases, more than one minute) is necessary. If a photo-induced structural change does not revert to an initial structure within the repetition period (946 Hz = 1.06 ms), this target species is almost saturated in the sample crystal and its observation should be performed using the snapshot method. When a target photo-induced species is perfectly deactivated within the repetition period, the stepwise molecular dynamics can be observed by the stepwise change of exposure timing of the laser pulse and the X-ray pulse.

Diffraction data sets at the laser-irradiated and non-irradiated conditions should be collected to clarify any small photo-induced structural changes by subtraction analysis. Minimizing the systematic errors between the data sets is important because the amount of photo-induced species in a crystal is small and can be veiled by these errors. In the present experiment, each diffraction image at the laser-irradiated and non-irradiated conditions were alternatively collected to minimize systematic errors; in the case of a 1° oscillation for one data frame, 0 to 1° oscillation image in the laser-irradiated condition → 0 to 1° oscillation image in the non-irradiated condition → 1 to 2° oscillation image in the laser-irradiated condition → 1 to 2° oscillation image in the non-irradiated condition, and likewise. Damage by laser-irradiation on the sample crystal should be suppressed as far as possible, but may be accumulated in the pump-probe spectroscopic or X-ray experiment. The above alternative data collection is required for applying the pump-probe technique to single crystal X-ray structural analysis.

Observation of photocatalyst at a photo-excited state and geometrical rearrangement

One of the organic photocatalysts, 9-mesityl-10-methylacridinium (Acr^+–Mes, Fig 2), is a molecule in which an

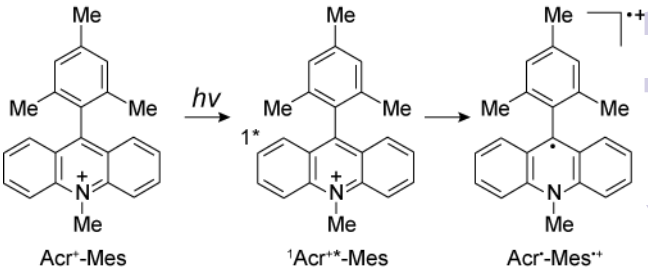

Fig. 2 Schematic drawing for representing photo-induced process of Acr^+–Mes. Reprinted with permission from Ref. 14. Copyright (2011) American Chemical Society.

electron donor (mesitylene; Mes) and an acceptor (acridinium cation; Acr^+) are directly connected by a covalent bond.[18] Steric hindrance between Acr^+ and Mes causes them to be arranged perpendicularly and the LUMO and HOMO of Acr^+–Mes are localized near to each other.[18] Singlet-excited Acr^+ ($^1Acr^{+*}$) is generated by the absorption of visible light and reaches the electron-transfer (ET) state within about 5 ps after generation of $^1Acr^{+*}$–Mes. This ET state has an extremely long lifetime at low temperatures (2 hours at 203 K and almost infinity at 77 K). The energy of this ET state is reported as 2.37 eV, which is beyond the photosynthetic reaction center at the charge-separated state. Various photocatalytic reactions exhibiting such properties have been reported.[19,20]

Direct observation of the photo-induced structural dynamics in the crystal of Acr^+–Mes(ClO_4^-) established the above photochemical properties of Acr^+–Mes. In the pump-probe X-ray diffraction experiment, excitation pulsed laser light (λ = 4[illegible]5 nm, 8 mJ cm^{-2}) is irradiated to the sample crystal just before exposure to the X-ray pulse. A typical time-resolution of the X-ray pulse is about 100 ps. Therefore, X-ray crystal structure analysis is unable to capture the time-averaged structure in the crystal for approximately 100 ps after excitation under these conditions. X-ray crystallographic observation using a characteristic differential Fourier map, a photo-difference Fourier map[21,22] was performed. This map is drawn using the difference of observed structural factors (F_o) between the laser-irradiated (on) and non-irradiated (off) conditions [$F_{o(on)} - F_{o(off)}$]. In this map, the electron densities with the initial distributions are subtracted and some slightly deformed

densities caused by the photo-excitation are highlighted. Examples of differential electron densities representing photo-induced geometrical or electronic changes are shown in Fig. 3.

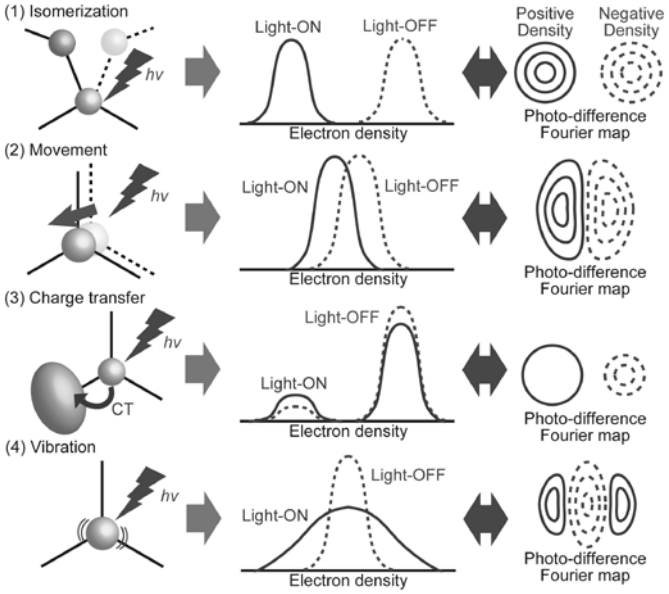

Fig. 3 Typical examples for differential electron densities in the photo-difference Fourier map. Reprinted with permission from Ref. 23. Copyright (2014) The Crystallographic Society in Japan.

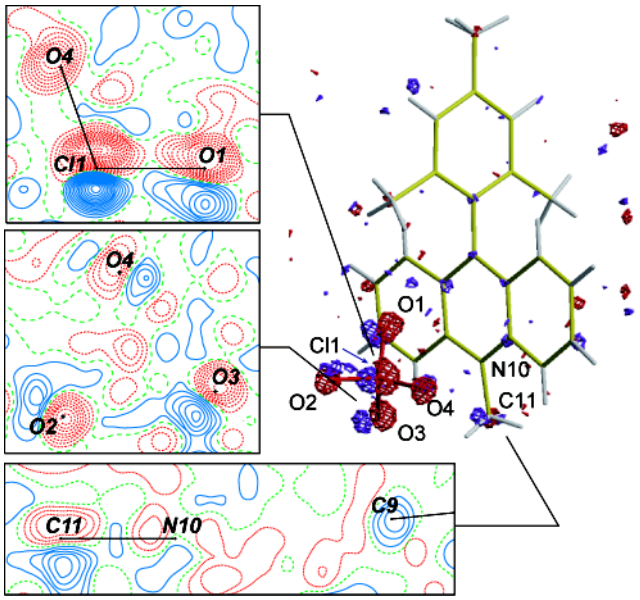

Fig. 4 Photo-difference Fourier map describing structural change by photo-excitation in Acr^+–$Mes(ClO_4^-)$, with a contour interval of 0.03 e $Å^{-3}$ and ±0.1 e $Å^{-3}$ isosurfaces. Blue, red, and green colored lines and surfaces denote positive, negative, and zero electron densities, respectively. Reprinted with permission from Ref. 14. Copyright (2011) American Chemical Society.

The photo-difference Fourier map of Acr^+–$Mes(ClO_4^-)$ is shown in Fig. 4. Difference electron densities around the methyl group in Acr^+ represented bending by photo-excitation. Theoretical calculations for describing the electron configurations in Acr^+ explain that bending of the methyl group changes the orbital hybridization from sp^2 to sp^3 around the nitrogen atom accompanying electron acceptance and reduction. Drawing the free space for this bending in the crystal demonstrates that the geometrical change by photo-excitation proceeds towards the spatially favorable direction by avoiding steric repulsion (Fig. 5a). This bending makes the vacancy,

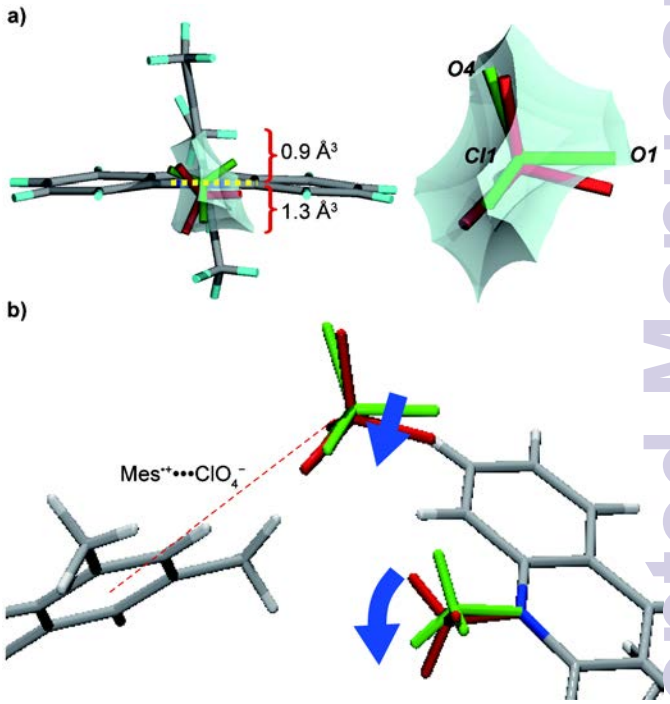

Fig. 5 Photo-induced geometrical changes with the surrounding environment. Green and red fragments represent the geometry before and after photo-excitation. (a) Drawing of the free space for geometrical change in the crystal. The space is represented as a greenish-blue area. (b) Selected area for representing co-operative geometrical change owing to the formation of the E state. Blue arrows represent the direction of the geometrical change and the red-dotted line indicates an intermolecular interaction. Reprinted with permission from Ref. 14. Copyright (2011) American Chemical Society.

which leads to the co-operative stepwise structural rearrangement in the crystal. The photo-difference Fourier map and drawing of the free space[24] around ClO_4^- in the crystal showed that ClO_4^- was moved in a spatially unfavorable direction by photo-excitation (Fig. 5a). However, the vacancy created by the bending of the methyl group by photo-excitation accepts the movement of ClO_4^-. The driving force for this movement is the electrostatic interaction between ClO_4^- and the electron-donated and positively-charged Mes because the direction of this movement is toward the closest Mes moiety in the crystal (Fig. 5b). The observed structural change in Acr^+–$Mes(ClO_4^-)$ established photo-induced electron donation and acceptance in Mes and Acr^+ (i.e., generation of the ET state) together with representing the molecular dynamics which commences after formation of the ET state, through bending of the methyl group, and competes with the movement of ClO_4^-.

Consideration for the development from snapshot observation to stepwise observation

Stepwise structural change by photo-excitation in Acr^+–$Mes(ClO_4^-)$ is estimated by snapshot observation of the crystal structure just after photo-excitation using pump-probe X-ray crystal structure analysis. This observation is completed within the time duration of an X-ray pulse (about 100 ps). In the case of rather slow dynamics (e.g., in the nanosecond or hundreds of picoseconds range), temporal structural changes will be visualized in a 'frame-by-frame' fashion by a stepwise timing delay of the X-ray pulse after the excitation pulsed laser light in the pump-probe X-ray crystal structure analysis. Collecting X-ray diffraction data sets for all delay conditions without changing the sample is necessary to avoid the introduction of systematic errors between the data sets. Consideration of damage on the sample crystal by laser irradiation should be given. Accumulation of damage degrades the quality of the diffraction data and makes crystallographic analysis of a photo-excited molecular structure difficult. The effects of damage accumulation in pump-probe X-ray crystallographic analysis were evaluated through the study on the photo-excited structure of Acr^+–$Mes(ClO_4^-)$. The laser power dependence on the photo-difference Fourier map of Acr^+–$Mes(ClO_4^-)$ was validated under the excitation power settings of 2, 4, 6, 8, 10, and 12 mJ cm^{-2}. The photo-difference Fourier maps around the ClO_4^- ion under the above conditions are shown in Fig. 6. The

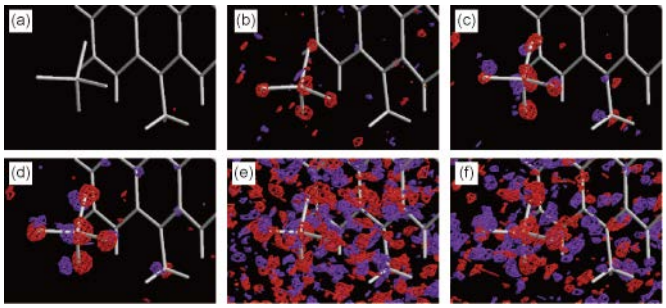

Fig. 6 Laser power dependence on the photo-difference Fourier map of Acr^+–$Mes(ClO_4^-)$ with ±0.1 e $Å^{-3}$ isosurfaces (blue: positive, red: negative). Power was set as (a) 2, (b) 4, (c) 6, (d) 8, (e) 10, and (f) 12 mJ cm^{-2}.

contrast between positive and negative electron density in the map became high by increasing laser power from 2 to 8 mJ cm^{-2}. However, for 10 or 12 mJ cm^{-2} excitation, an increase of the noise in the electron densities was observed that obscured the differential electron densities concerned with the structural change by photo-excitation. This dependence indicates the importance of selecting a suitable power of excitation photon for minimizing the laser irradiation damage.

Stepwise observation of TTF-CA in a deactivation process of PIPT

Direct observation of the stepwise photo-induced structural change using pump-probe X-ray crystal structure analysis was performed in the study on photo-induced phase transition (PIPT) of a co-crystal of tetrathiafulvalene and *p*-chloranil (TTF-CA, Fig. 7a and b).[25] A charge-transfer interaction between TTF and CA accompanied with an electron-lattice interaction are observed in the crystal and dominates the character of the quasi-neutral (N phase, degree of charge-

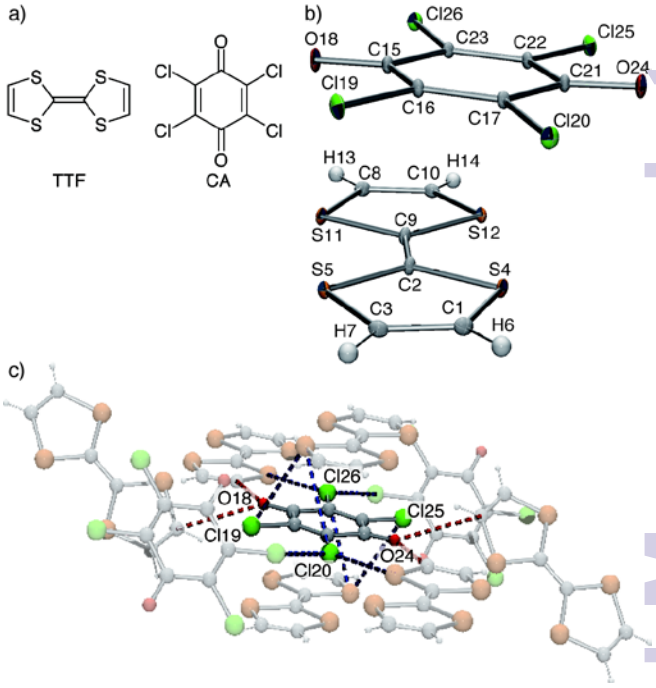

Fig. 7 (a) Chemical structure and (b) ORTEP diagram of TTF-CA. (c) Weak Cl···S and Cl···Cl interactions (blue-dotted lines) and C–H···O hydrogen bonds (red-dotted lines) in TTF-CA. Reproduced from Ref. 15 with permission from The Royal Society of Chemistry.

transfer $\rho \sim 0.3$) and the quasi-ionic (I phase, $\rho \sim 0.7$) phases. The phase of TTF-CA depends on the temperature; the N phase at temperatures above $T_c = 81$ K and the I phase at temperatures below T_c.[26] PIPT of TTF-CA from the N to I phase takes place with short-pulsed laser irradiation ($\lambda = 800$ nm) around 90 K. PIPT from the I to N phase is observed at temperatures below T_c. PIPT from the N to I phase at 90 K is completed almost instantaneously with laser irradiation and recovered to the initial N phase within 20 ps after irradiation at a weak excitation condition (power density of excitation laser is less than 10 mJ cm^{-2}).[27] Moreover, a recent ultrafast spectroscopic study indicated the existence of another phase observed at hundreds of picoseconds after PIPT.[28] In this study, the ρ of this phase was suggested to be lower than the one at the initial phase (i.e., over-neutralized).

Detailed observation of the structural features in this crystal is required to characterize this unique phase. Especially, dynamic structural deformation in the crystal before reaching this phase would provide the mechanism describing the dominant factors for its construction. As already described above, optimizing the excitation power of light for minimizing systematic errors should be performed to observe stepwise structural deformation using pump-probe X-ray crystal structure analysis. The experimental conditions of pump-probe spectroscopy would be helpful for selecting a suitable excitation power. If a characteristic signal appearing with laser excitation in a spectrum gradually decreases with time, it can be attributed to damage by laser irradiation with excessive power that is accumulated in the sample crystal. In the case of TTF-CA, the pump-probe spectroscopic study for this over-neutralized phase with less than 10 mJ cm^{-2} laser power has already been reported elsewhere.[27,28] Iterative data accumulation over a whole day, to satisfy significant signal-to-noise ratio in that

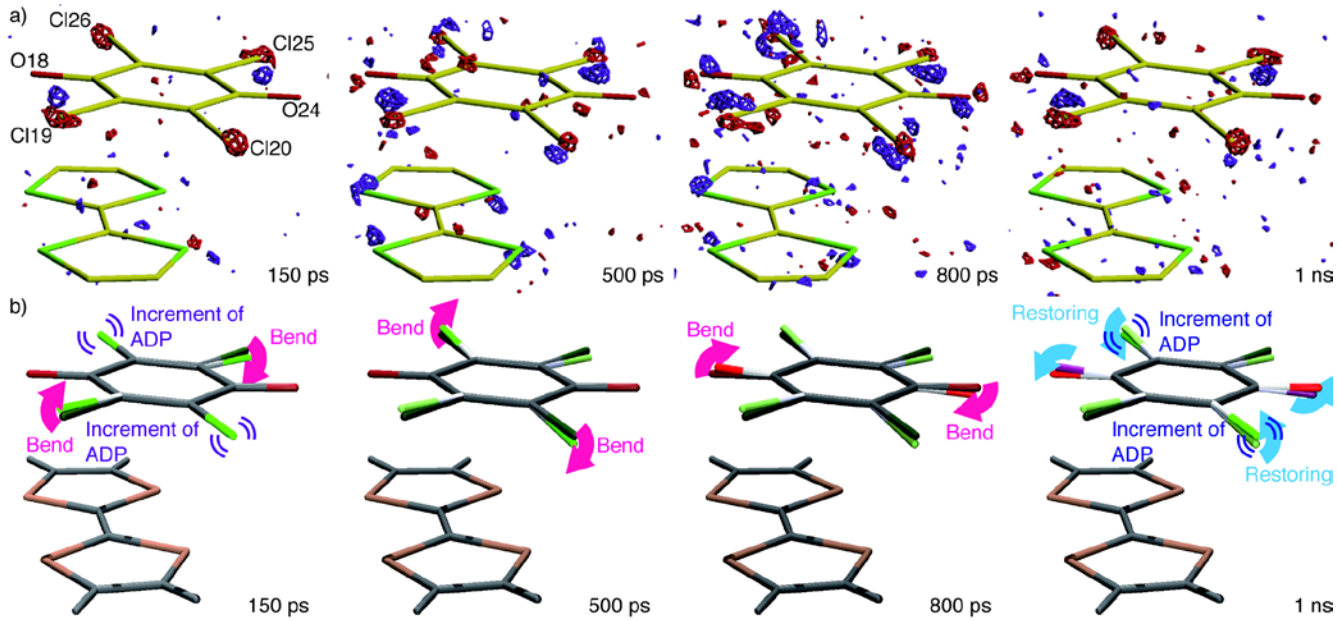

Fig. 8 Photo-difference Fourier maps representing stepwise photo-induced structural deformation in TTF-CA at 90 K. Positive (blue) and negative (red) electron densities are drawn using ±0.1 e Å^{-3} isosurfaces. Reproduced from Ref. 15 with permission from The Royal Society of Chemistry.

spectrum, is acceptable under these excitation conditions. From these observations, the pump-probe X-ray diffraction experiment with suitable excitation power (< 10 mJ cm^{-2}) was designed for dynamic observation in the TTF-CA crystal.

Characteristic over-neutralization relating to relaxation of intermolecular interactions

The power density of the femtosecond pulsed laser (λ = 800 nm) for excitation was tuned to 8 mJ cm^{-2}. The X-ray pulse was delayed by 150 ps, 500 ps, 800 ps, and 1 ns after the laser pulse at the sample position. The photo-difference Fourier map drawings using the data collected at 90 K (Fig. 8) represented a gradual change of electron densities around CA with time. When the delay (Δt) was 150 ps, the differential electron densities around two Cl atoms (labeled as Cl19 and Cl25) were represented as bending at a C–Cl bond toward the phenyl ring. Around the other Cl atoms (Cl20 and Cl26), their vibration was suggested in the map. When the delay was increased to 500 ps, Cl19 and Cl25 still remained in the bent position and Cl20 and Cl26 moved to represent bending of their bonds. The bonding of the four C–Cl bonds was maintained at Δt = 800 ps. At this delay time, the positional change of O18 and O24 is represented in the map. The differential electron density at Δt = 1 ns was similar with that at Δt = 150 ps. This observation represented that Δt = 800 ps is the time when the expected over-neutralized phase is formed and Δt = 1 ns is during the deactivation pathway to the initial phase. Structural deformation at Δt = 800 ps is evaluated in detail by drawing the two-dimensional photo-difference Fourier map in the mean plane of CA (Fig. 9a). The pair of positive and negative electron densities around O18 and O24 represent that the positional changes of O18 and O24 was a result of the shortening of C=O bonds. The reported distribution of molecular orbitals[29] explains that shortening of the C=O bonds in CA corresponds to the suppression of antibonding character

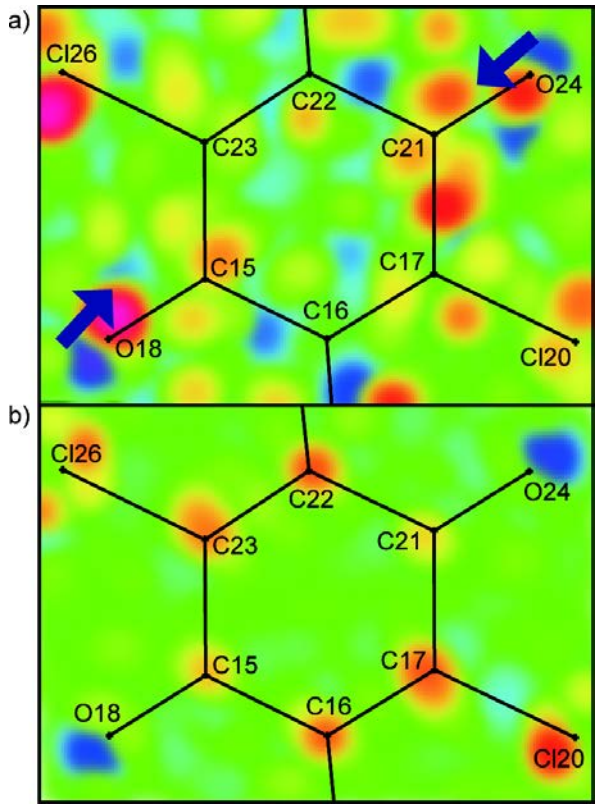

Fig. 9 (a) Photo- and (b) thermal-difference Fourier maps along the mean plane of CA. Max(red)/min(blue) = 0.10/−0.10 eÅ^{-3} in (a) and 0.20/−0.55 eÅ^{-3} in (b). Delay condition corresponding to (a) is 800 ps. The arrows in (a) indicate shortening of C=O bonds by photo-excitation. Reproduced from Ref. 15 with permission from The Royal Society of Chemistry.

of the LUMO in CA and represents back-charge transfer from CA to TTF, that is, decrement of ρ, in the crystal. These C=O bond shortenings were examined by the comparison with the map described using the coefficient of $[F_{o(100\ K)} - F_{o(90\ K)}]$ at the non-irradiated condition (the thermal-difference Fourier map; Fig. 9b). The change of length in C=O was not represented in this map and, therefore, the photo-induced C=O shortening originated from the photo-excitation. The difference of lattice expansion by photo-irradiation (within +0.5 Å^3) and 10 K heating (ca. +2 Å^3) suggests that the increment of the sample temperature with laser irradiation is less than 10 K. Hence, the phase of TTF-CA at Δt = 800 ps is definitely the over-neutralized phase and this phase is unique in the photo-induced process, rather than in the thermal process.

It is notable that the formation mechanism of this over-neutralized phase was proposed as a stepwise relaxation of the intermolecular interactions in the crystal. From a previous study on the strength of the intermolecular interactions in TTF-CA by topological X-ray crystal structure analysis,[30] the potential energy densities of the intermolecular interaction around CA (shown in Fig. 7c) are approximately 8 kJ mol^{-1} for the weak intermolecular interactions (Cl···S and Cl···Cl) and approximately 20 kJ mol^{-1} for the C–H···O hydrogen bonds. The Cl atoms are stabilized by Cl···S and Cl···Cl. These weak interactions are expected to relax immediately in the deactivation process from PIPT. Therefore, positional changes of these atoms occurred at Δt = 150 ps. Meanwhile, the O atoms are stabilized by the relatively strong intermolecular interactions. Therefore, a longer retention time until their positional change (Δt = 800 ps) compared with Cl atoms was recorded. The environment around the Cl19 and Cl25 is different from that around Cl20 and Cl26. The former two Cl atoms are stabilized by one Cl···S interaction. However, the latter two C1 atoms are stabilized by two Cl···S interactions and one Cl···Cl interaction. These three intermolecular interactions result in the deformation of the potential surface by their relaxation complex, and so change of the differential electron density from vibration (Δt = 150 ps) to bending (Δt = 500 ps) was observed in the photo-difference Fourier maps. A schematic of the time course describing this different relaxation process is depicted in Fig. 10.

Relaxation of intermolecular interactions could be considered as the reduction of internal pressure in TTF-CA. Indeed, the ρ of TTF-CA is decreased by reducing the pressure.[31] The observed stepwise relaxation of intermolecular interactions represents the working process of the photo-induced negative pressure effect leading to over-neutralization.

Thermal dynamics in the crystal of an azobenzene derivative showing PCMT

To observe the photo-induced dynamics using pump-probe X-ray crystallography, obtaining the precise differences of the diffraction intensities to draw the photo-difference Fourier map representing geometrical changes of the molecule is essential. Precise data are also important for the observation of the thermal dynamics of molecules by X-ray crystallography. However, the precise intensities themselves, rather than the difference of intensities, is required to determine the thermal dynamics.

The crystal of a methylene-bridged *trans*-azobenzene dimer possessing four long methoxy chains (*trans*/*trans*-**1**, Fig. 11a), shows melting by photo-irradiation, termed as the photo-induced crystal-melt transition (PCMT, Fig. 11b and c).[32,33] This molecule is designed for showing PCMT by large conformational change owing to *trans-cis* photoisomerization

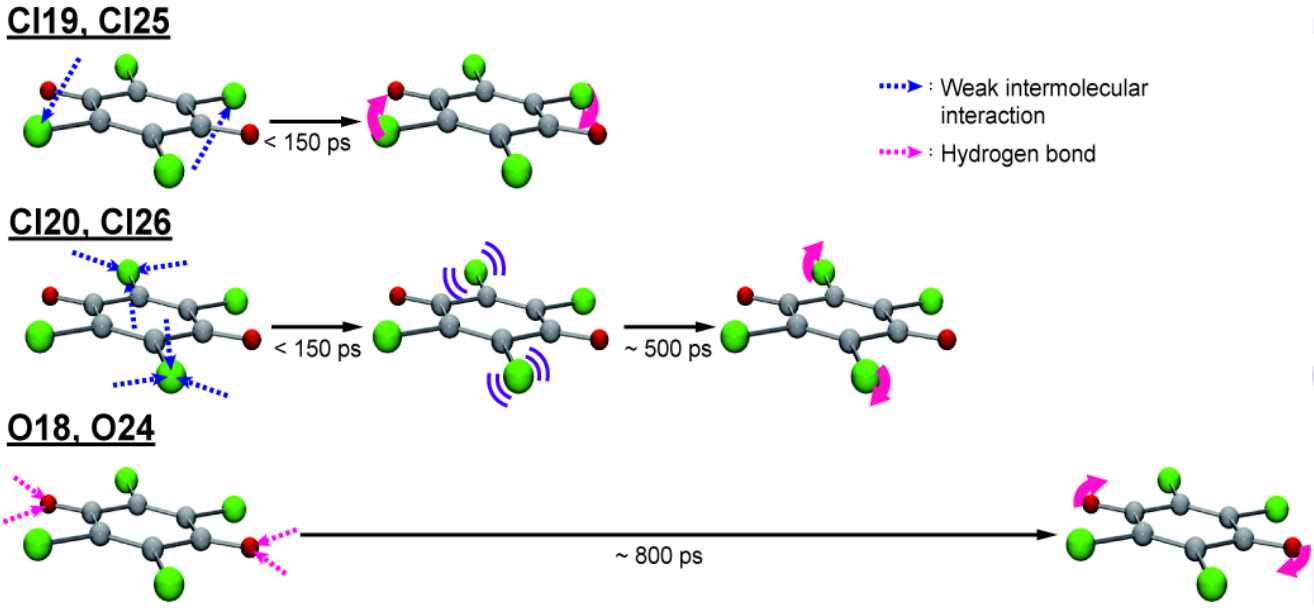

Fig. 10 Schematic of the time course for the stepwise geometrical change in CA observed by pump-probe single crystal X-ray structural analysis. Bold arrows and double arc lines indicate atomic movement and vibration, respectively.

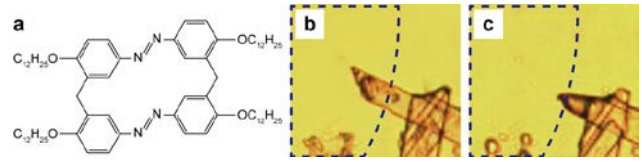

Fig. 11 (a) Chemical structure of *trans*/*trans*-**1**. (b,c) Microscopic observation of its PCMT. Reprinted with permission from Ref. 16. Copyright (2014) American Chemical Society.

and decomposition of the expected π···π stacking together with this isomerization. Therefore, the structural features (possibility for *trans*-*cis* photoisomerization of azobenzene moieties and their π···π stacking) of *trans*/*trans*-**1** would provide a solid basis for this drastic morphology change. However, X-ray diffraction of the powdered crystal of *trans*/*trans*-**1**, using an in-house X-ray diffractometer, shows only a few diffractions possessing significant intensities at the low-angle region.[32] This result suggests that dynamic disorder is contained in this crystal and this disorder is expected to dominate PCMT. To improve the diffraction intensity from the crystal of *trans*/*trans*-**1** at the high-angle region, synchrotron X-rays from an undulator device were used for the single crystal X-ray diffraction experiment. Owing to the strong X-rays from the synchrotron, a suitable resolution of X-ray diffraction data (more than 1 Å) for structural analysis could be obtained. The thermal dynamic nature of *trans*/*trans*-**1** was evaluated by consideration of the temperature dependence on the crystal structure. ORTEP diagrams at all temperatures (Fig. 12) show that the long methoxy chains in *trans*/*trans*-**1** begin thermal motion accompanied by their conformational change between 190 and 240 K during the heating process. These temperatures are the same as those for PCMT. The temperature dependence of

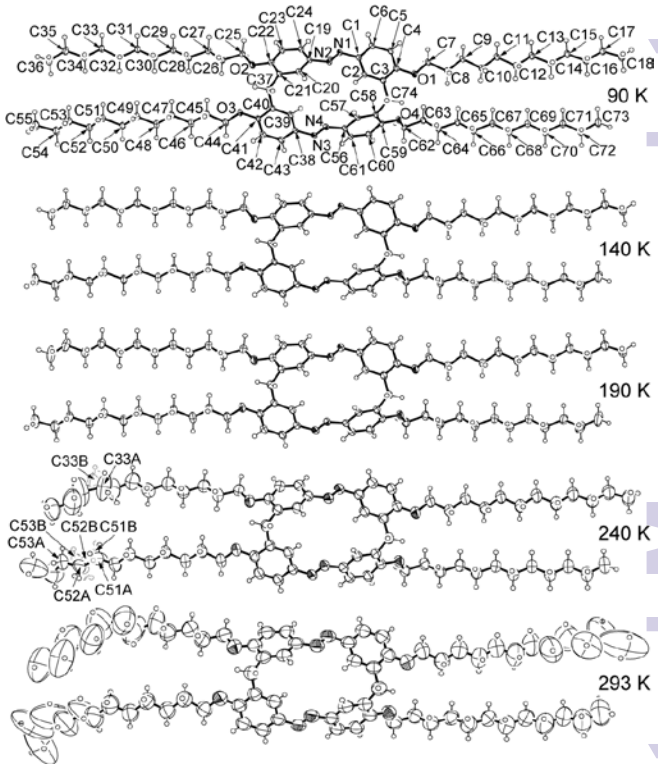

Fig. 12 ORTEP diagrams of *trans*/*trans*-**1** at all measured temperatures. Reprinted with permission from Ref. 16. Copyright (2014) American Chemical Society.

PCMT was considered by the variable temperature powder X-ray diffraction experiment (Fig. 13). The temporal change of the strongest Bragg reflection under the continuously photo-

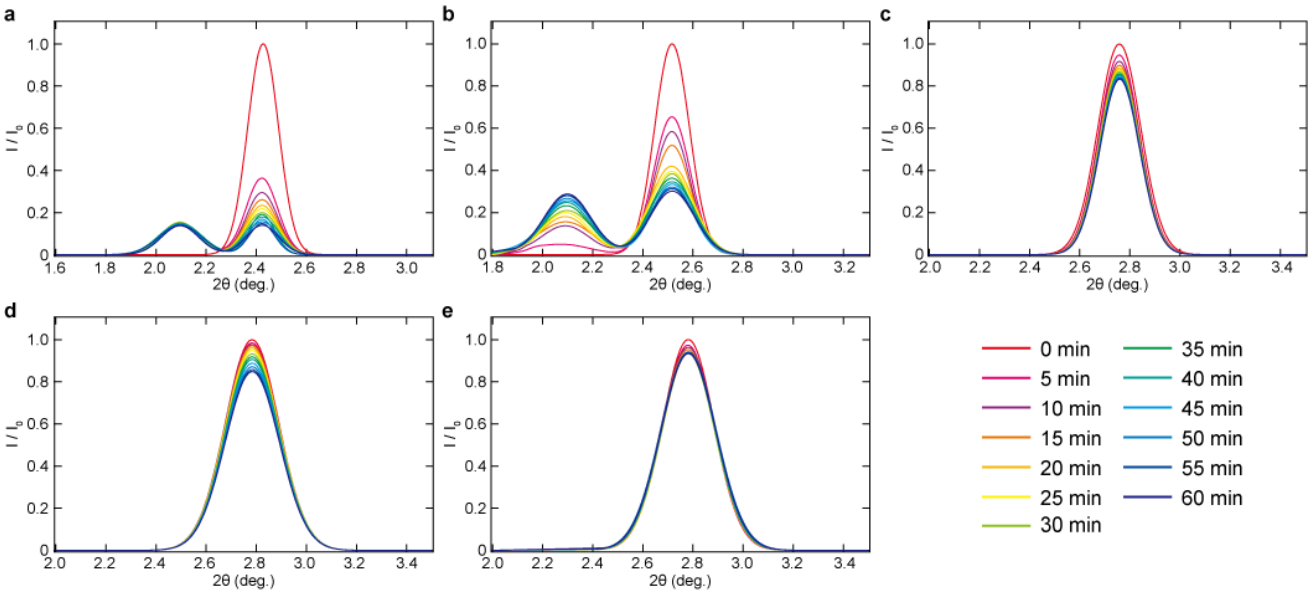

Fig. 13 Temporal change of selected diffraction intensities from powdered *trans*/*trans*-**1** under UV irradiation. Measurement temperatures are (a) 293, (b) 240, (c) 190, (d) 140, and (e) 90 K. Reprinted with permission from Ref. 16. Copyright (2014) American Chemical Society.

irradiated condition (λ = 365 nm, LED was used as a light source) was studied. At 240 and 293 K, generation of the new reflection was observed within 5 minutes after the start of photo-irradiation. This new reflection corresponded to the X-ray diffraction from the crystalline phase of mainly photo-isomerized *cis*/*cis*-**1**, grown from the melt phase after PCMT and characterized by UV/Vis absorption spectroscopy.[32] These data elucidate that PCMT appeared at 240 and 293 K, at which temperatures the thermal motion accompanying conformational change of the long methoxy chains were found in the crystal (Fig. 12). This consistency indicates that dynamic disorder of the long methoxy chains are required for showing PCMT. Thermal dynamics of the long methoxy chains lead to the rearrangement of the crystal packing in *trans*/*trans*-**1**. The packing motif containing four selected molecules at all temperatures (Fig. 14a) represents molecular rotation led by intermolecular π···π interactions, which commenced between 190 and 240 K. Indeed, the distance of π···π interactions (R2, described in Fig. 14b) between Ph1s shortened from approximately 5.9 to 3.7 Å by heating from 90 to 293 K. This is a sacrifice phenomenon describing substitute formation of π···π interactions arising from significant weakening of many alkyl···π and alkyl···alkyl interactions by the thermal motion. Crystal packing after the formation of the above intermolecular π···π interactions contains one-dimensional π stacking, which is expected to show PCMT. Hence, thermal dynamics leads to the transformation of the crystal structure of *trans*/*trans*-**1** from a tightly interacted crystal at low temperature to a loosely packed crystal with one-dimensional stacking by intermolecular π···π interactions at high temperature. The latter packing fashion is essential for PCMT.

Rationalization of PCMT using a two-component phase diagram

The photochemical phase transition has four classifications based on periodicity and morphology.[34,35] The first is the transition to an equivalent stable crystalline phase, which has the same periodicity and is formed without crystal deterioration.[36,37] The second is the transition to an equivalent metastable crystalline phase. This phase has the same periodicity, but deterioration from a single crystalline state to a polycrystalline state occurs in this transition process.[38] The third is the transition to a new stable phase. In this transition, the periodicity alternation takes place with crystal deterioration.[39] The last is the transition to an isotropic phase, such as amorphous[34] or melt phase.[40] This transition loses periodicity in the starting material and, in some cases, alters its appearance. It should be noted, all the transitions should commence with formation of the solid-solution phase, in which small amount of photo-reacted species are mixed without lattice deformation.[34,35]

The three phenomena described above can be involved in the photochemical phase transition. The ET state of Acr^{+}–Mes was observed in a solid-solution phase, a precursor phase in the

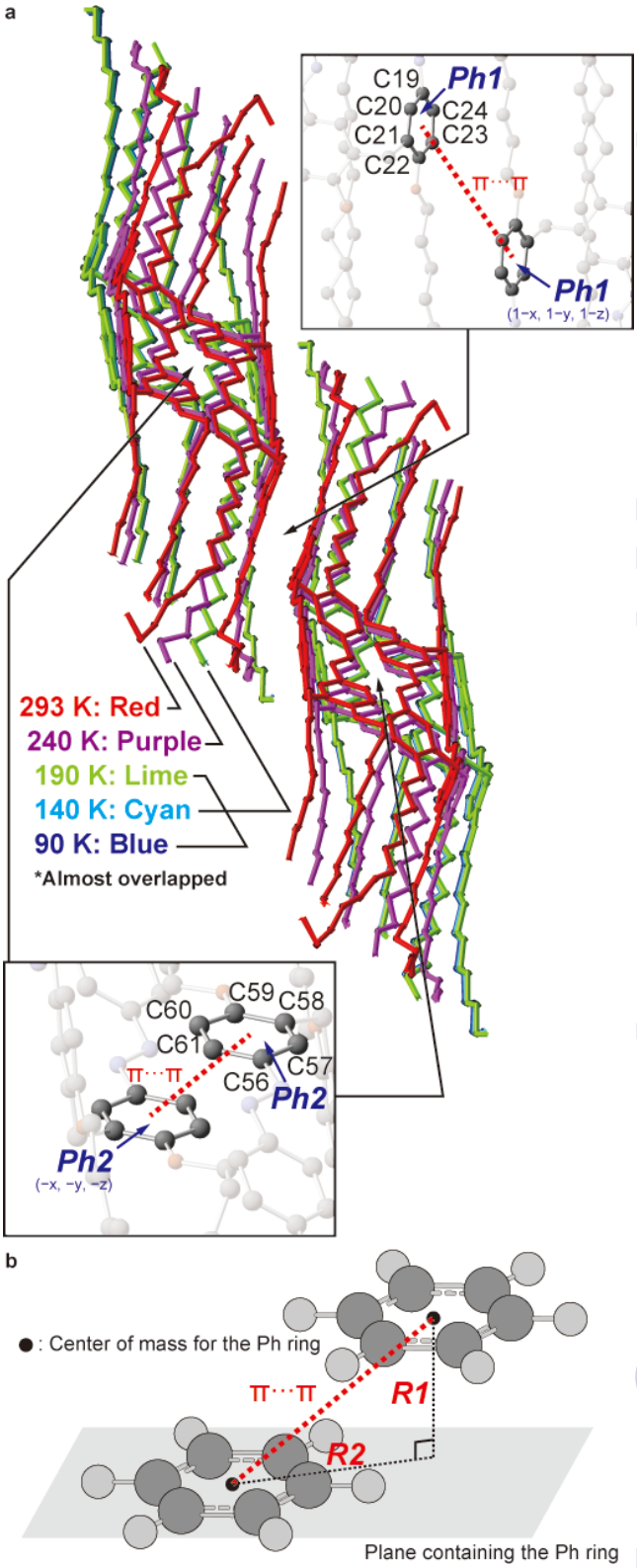

Fig. 14 (a) Overlapped packing motif in *trans*/*trans*-**1**. The red dotted lines represent the π···π interactions. (b) Definition of R1 and R2 for evaluating the strength of the π···π interaction. Reprinted with permission from Ref. 16. Copyright (2014) American Chemical Society.

photochemical phase transition. Indeed, the population of the ET state species in this crystal was estimated as 2%.[14] This population could be increased by exposure to a more intense excitation source. However, population improvement of the ET state of Acr^+–Mes leads to the deterioration of the crystal by co-operative geometrical rearrangement in the crystal. This deterioration is expected from the study on the laser power dependence, shown in Fig. 6. PIPT of TTF-CA is classified in the transition to the same stable phase. The geometrical change in this process is not drastic and so its crystallinity is maintained. This type of transition with reversibility is suitable for observing the molecular dynamics by pump-probe X-ray crystallography. Optimizing the excitation condition to achieve a reversible transition between an initial and a photo-induced phase without crystal deterioration is required for observation of the molecular dynamics.

Thermal dynamics in *trans*/*trans*-**1** alters the transition pathway, which is classified in the transition to an isotropic phase. The two-component phase diagram (Fig. 15), as a function of

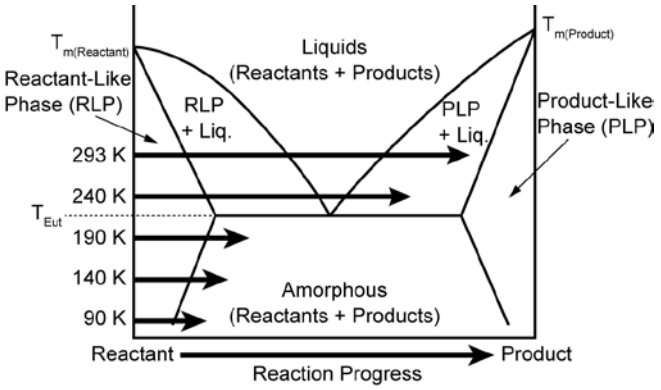

Fig. 15 Two-components phase diagram describing the photochemical transition of *trans*/*trans*-**1**. Arrows represent the transition pathway confirmed by powder X-ray diffraction under photo-irradiation. Reprinted with permission from Ref. 16. Copyright (2014) American Chemical Society.

photoreaction progress, was determined. In the case where the thermal dynamic motion was suppressed at low temperatures (190, 140, 90 K), PCMT was not observed and partial amorphization was confirmed by observation of a slight decrement of the X-ray diffraction intensity by photo-irradiation. Thermal dynamic motion in the long methoxy chains at 240 and 293 K alters the intermolecular interactions in *trans*/*trans*-**1** to satisfy crystal-packing features for overcoming PCMT. Powder X-ray diffraction from the crystalline phase of mainly *cis*/*cis*-**1**, appearing after photoirradiation, represents that the phase transition can progress beyond the liquid (PCMT) phase and result in the mixture of the product-like phase and the liquid phase.

Conclusions

Observation of the molecular dynamics by crystallographic analysis was achieved by studies using synchrotron X-rays. The co-operative rearrangement of molecules in Acr^+–$Mes(ClO_4^-)$ represented the electronic features of the ET state of Acr^+–Mes. The structure of this state is deeply involved in the function of Acr^+–Mes as a photocatalyst. The observed structure is informative as a scaffold for designing an efficient solar energy conversion system. Stepwise molecular deformation in TTF-CA in the deactivation process of PIPT revealed a characteristic phase for the first time. Recently, investigation of the molecular dynamics using a shorter pulsed electron beam[41] or X-ray[42] have been reported elsewhere. The present pump-probe X-ray crystallography suggests its feasibility for crystal structure analysis of ultrafast dynamics using short-pulsed light sources. Thermal dynamics in the crystal of *trans*/*trans*-**1** were also successfully observed using high intensity synchrotron X-rays. This dynamic movement alters its properties as a bulk material and enables PCMT. As shown in the present studies, the observation of molecular dynamics improves understanding about the features of phases of a material. Three-dimensional geometrical change in a molecule and a molecular aggregation is beneficial for application as more sophisticated functional materials.

Acknowledgements

This work was approved by the Photon Factory Program Advisory Committee (PF-PAC Nos. 2009S2-001, 2009G626, 2011G591, and 2013G607).

Notes and references

[a] Department of Chemistry and Materials Science, Tokyo Institute of Technology and CREST-JST, Meguro-ku, Tokyo 152-8551, Japan.
[b] Photon Factory, High Energy Accelerator Research Organization and PRESTO-JST, Tsukuba, Ibaraki 305-0801, Japan.
*Present address (M.H.): Department of Applied Chemistry, Graduate School of Engineering, The University of Tokyo, 7-3-1 Hongo, Bunkyo-ku, Tokyo 113-8656, Japan. Fax:+81 3 5841 0357; Tel: +81 3 5841 0357; E-mail: mhoshino@appchem.t.u-tokyo.ac.jp.

1 P. Coppens, *J. Phys. Chem. Lett.*, 2011, **2**, 616.
2 J. Hallmann, W. Morgenroth, C. Paulmann, J. Davaasambuu, Q. Kong, M. Wulff, and S.Techert, *J. Am. Chem. Soc.*, 2009, **131**, 1501[illegible].
3 E. Collet, M. H. Lemée-Cailleau, M. Le Cointe, H. Cailleau, M. Wulff, T. Luty, S. Koshihara, M. Meyer, L. Toupet, P. Rabiller and S. Techert, *Science,* 2003, **300**, 612.
4 J. M. Cole. *Chem. Soc. Rev.*, 2004, **33**, 501.
5 P. Coppens, B. Ma, O. Gerlits, Y. Zhang and P. Kulshrestha, *CrystEngComm.*, 2002, **4**, 302.
6 S. Techert, F. Schotte, and M. Wulff, *Phys. Rev. Lett.*, 2001, **86**, 20[illegible].
7 C. D. Kim, S. Pillet, G. Wu, W.K. Fullagar and P. Coppens, *Acta Crystallogr. Sect. A*, 2002, **58**, 133.
8 S. Nozawa, S. Adachi, J. Takahashi, R. Tazaki, L. Guérin, M. Daimon, A. Tomita, T. Sato, M. Chollet, E. Collet, H. Cailleau, S. Yamamoto, K. Tsuchiya, T. Shioya, H. Sasaki, T. Mori, K.

Ichiyanagi, H. Sawa, H. Kawata and S. Koshihara, *J. Synchrotron Rad.,* 2007, **14**, 313–319.
9 P. Naumov, *Top. Curr. Chem.*, 2012, **315**, 111.
10 P. Coppens, O. Gerlits, I. I. Vorontsov, A. Yu. Kovalevsky, Y.-S. Chen, T. Graber and I. V. Novozhilova, *Chem. Commun.*, **2004**, 2144.
11 I. Vorontsov, T. Graber, A. Kovalevsky, I. Novozhilova, M. Gembicky, Y.-S. Chen and P. Coppens, *J. Am. Chem. Soc.*, 2009, **131**, 6566.
12 P. Naumov, N. Yasuda, W. M. Rabeha and J. Bernstein, *Chem. Commun*., 2013, **49**, 1948.
13 N. Yasuda, H. Murayama, Y. Fukuyama, J. Kim, S. Kimura, K. Toriumi, Y. Tanaka, Y. Moritomo, Y. Kuroiwa, K. Kato, H. Tanaka and M. Takata, *J. Synchrotron Rad.*, 2009, **16**, 352.
14 M. Hoshino, H. Uekusa, A. Tomita, S. Koshihara, T. Sato, S. Nozawa, S. Adachi, K. Ohkubo, H. Kotani and S. Fukuzumi, *J. Am. Chem. Soc.,* 2012, **134**, 4569.
15 M. Hoshino, S. Nozawa, T. Sato, A. Tomita, S. Adachi and S. Koshihara, *RSC Adv.*, 2013, **3**, 16313.
16 M. Hoshino, E. Uchida, Y. Norikane, R. Azumi, S. Nozawa, A. Tomita, T. Sato, S. Adachi, S. Koshihara, *J. Am. Chem. Soc.*, 2014, **136**, 9158.
17 M. Hoshino, *J. Surf. Sci. Soc. Jpn.*, 2013, **34**, 598 (*in Japanese*).
18 S. Fukuzumi, H. Kotani, K. Ohkubo, S. Ogo, N. V. Tkachenko and H. Lemmetyinen, *J. Am. Chem. Soc.*, 2004, **126**, 1600.
19 S. Fukuzumi, K. Doi, A. Itoh, T. Suenobu, K. Ohkubo, Y. Yamada and K. D. Karlin, *Proc. Natl. Acad. Sci. U.S.A.*, 2012, **109**, 15572.
20 H. Kotani, K. Ohkubo and S. Fukuzumi, *J. Am. Chem. Soc.*, 2004, **126**, 15999.
21 M. D. Carducci, M. R. Pressprich and P. Coppens, *J. Am. Chem. Soc.,* 1997, **119**, 2669.
22 Y. Ozawa, M. R. Pressprich and P. Coppens, *J. Appl. Cryst*., 1998, **31**, 128.
23 M. Hoshino, *J. Cryst. Soc. Jpn.*, 2014, 56, 115 (*in Japanese*).
24 Y. Ohashi, K. Yanagi, T. Kurihara, Y. Sasada and Y. Ohgo, *J. Am. Chem. Soc.*, 1981, **103**, 5805.
25 S. Koshihara, Y. Takahashi, H. Sakai, Y. Tokura and T. Luty, *J. Phys. Chem. B,* 1999, **103**, 2592.
26 J. B. Torrance, A. Girlando, J. J. Mayerle, J. I. Crowley, V. Y. Lee and P. Batail, *Phys. Rev. Lett.,* 1981, **47**, 1747.
27 H. Okamoto, Y. Ishige, S. Tanaka, H. Kishida, S. Iwai and Y. Tokura, *Phys. Rev. B,* 2004, **70**, 165202
28 Y. Matsubara, Y. Okimoto, T. Yoshida, T. Ishikawa, S. Koshihara and K. Onda, *J. Phys. Soc. Jpn.,* 2011, **80**, 124711.
29 C. Katan, P. E. Blöchl, P. Margl and C. Koenig, *Phys. Rev. B,* 1996, **53**, 12112.
30 P. García, S. Dahaoui, C. Katan, M. Souhassou and C. Lecomte, *Faraday Discuss.,* 2007, **135**, 217.
31 H. Okamoto, T. Mitani, Y. Tokura, S. Koshihara, T. Komatsu, Y. Iwasa, T. Koda and G. Saito, *Phys. Rev. B,* 1991, **43**, 8224–8232.
32 E. Uchida, K. Sakaki, Y. Nakamura, R. Azumi, Y. Hirai, H. Akiyama, M. Yoshida and Y. Norikane, *Chem. Eur. J.*, 2013, **19***,* 17391.
33 Y. Norikane, Y. Hirai and M. Yoshida, *Chem. Commun.*, 2011, **47***,* 1770.
34 D. de Loeroa, A. Stopin, and M. A. Garcia-Garibay, *J. Am. Chem. Soc.,* 2013, **135**, 6626.
35 A. E. Keating and M. A. Garcia-Garibay, Photochemical Solid-to-Solid Reactions. In *Organic and Inorganic Photochemistry*; Ramamurthy, V., Schanze, K., Eds.; Marcel Dekker: New York, 1998; Vol. 2, pp 195−248.
36 Y. Ohashi, *Chem. Rec.,* 2013, **13***,* 303.
37 Y. Ohashi, *Crystallogr. Rev.*, 2013, **19:Sup.1***,* 2.
38 O. S. Bushuyev, A. Tomberg, T. Friščić and C. J. Barrett, *J. Am. Chem. Soc.,* 2013, **135***,* 12556.
39 F. Guo, J. Martí-Rujas, Z. Pan, C. E. Hughes and K. D. M. Harris, *J. Phys. Chem. C*, 2008, **112**, 19793.
40 Y. Okui and M. Han, *Chem. Commun.,* 2012, **48***,* 11763.
41 M. Gao, C. Lu, H. Jean-Ruel, L. C. Liu, A. Marx, K. Onda, S. Koshihara, Y. Nakano, X. F. Shao, T. Hiramatsu, G. Saito, H. Yamochi, R. R. Cooney, G. Moriena, G. Sciaini and R. J. D. Miller, *Nature*, 2013, **496**, 343.
42 K. H. Kim, J. G. Kim, S. Nozawa, T. Sato, K. Y. Oang, T. Kim, H. Ki, J. Jo, S. Park, C. Song, T. Sato, K. Ogawa, T. Togashi, K. Tono, M. Yabashi, T. Ishikawa, J. Kim, R. Ryoo, J. Kim, H. Ihee and S. Adachi, *Nature*, 2015, **518**, 385.